

**СВОЙСТВА КОНТРОЛИРУЕМОГО ГИДРОТЕРМАЛЬНОЙ СТРУКТУРОЙ  
ТРЕЩИННО-ПОЛОСТНОГО ДОЛОМИТОВОГО КОЛЛЕКТОРА  
И ЕГО ВЛИЯНИЕ НА РАСПРЕДЕЛЕНИЕ НЕФТИ И ВОДЫ:  
ИССЛЕДОВАНИЕ НА ПРИМЕРЕ НИЖНЕМЕЛОВОГО БАЙИНЧАГАНСКОГО ПРОГИБА  
(бассейн Эрлиан, Северный Китай)**

**Чжичэн Лэй<sup>1</sup>, Ваншуй Ху<sup>2</sup>, Хуайминь Сюй<sup>1</sup>, Бо Сюй<sup>3</sup>, Чунь Цао<sup>4</sup>, Чао Чэн<sup>3</sup>, Цюйлэй Чжу<sup>1</sup>**

<sup>1</sup> College of Geoscience, China University of Petroleum-Beijing, Beijing, China

<sup>2</sup> College of Geoscience, Yangtze University, Wuhan, Hubei, China

<sup>3</sup> CNOOC China Co., LTD. Shanghai branch development production, Shanghai, China

<sup>4</sup> CNOOC EnerTech-Drilling&Production Co, Data Processing Co. Zhanjiang, Guangdong, China

На исследуемой территории трещины и полости в исходном доломитовом коллекторе способствовали улучшению его физических свойств и влияли на распределение нефти и воды в верхнетенгерской свите (нижний мел) Байинчаганского прогиба в бассейне Эрлиан. Исходя из данных исследования ядра, анализа тонких срезов и фотокаротажа, трещинно-полостной коллектор был изначально развит в литоральной области вблизи крыла конседиментационного разлома. Трещины имели тектоническую и диагенетическую природу. Крутопадающие закрытые и открытые тектонические трещины были широко развиты в доломитовых аргиллитах, а пологие и сетчатые трещины формировались в ходе тектоногидротермального процесса и заполнялись гидротермальными минералами. Коллектор находился в низменности, поэтому при захоронении растворяющихся под давлением обломков пород в процессе диагенеза образовывались трещины. Межзерновые и внутризерновые поры, образующиеся в результате гидротермальной деятельности, развивались в основном в отложениях с высоким содержанием доломита. Исходя из температуры диагенеза доломита, определённой при углерод-кислородном изотопном анализе, первоначальные отложения претерпели многочисленные внедрения гидротермальных растворов, что привело к их доломитизации перед массовой миграцией углеводородов. Растворение органических кислот, образованных углеводородами после доломитизации, и неорганических кислот, образованных в процессе диагенеза растворимых минералов, способствовало развитию коллекторских свойств отложений. Высокая гетерогенность отложений, обусловленная их литологическим составом и системами трещин, привела к сложным взаимоотношениям между нефтью и водой. В результате возникло несколько состояний этих фаз: трещинно-полостная нефть, изолированная нефть, аккумулярированная нефть, изолированная вода и аккумулярированная вода. Исследования ядра позволили определить распределение нефти и воды в отложениях.

*Гидротермальный доломит, трещинно-полостной коллектор, распределение нефти и воды, Северный Китай, бассейн Эрлиан.*

**CHARACTERISTICS OF HYDROTHERMAL-STRUCTURE-CONTROLLED FRACTURE-VUG  
DOLOMITE RESERVOIR AND ITS INFLUENCE ON OIL-WATER DISTRIBUTION:  
A CASE STUDY ON THE LOWER CRETACEOUS, BAIYINCHAGAN SAG, ERLIAN BASIN, NORTH CHINA**

**Zhicheng Lei, Wangshui Hu, Huaimin Xu, Bo Xu, Chun Cao, Chao Cheng, and Qulei Zhu**

Fractures and vugs were used as the primary dolomite reservoir space in the study area, which improved the reservoir's physical properties and influenced the distribution pattern of oil and water that were developed in the Upper Tenger Formation, Lower Cretaceous, Baiyinchagan sag, Erlian Basin. Based on the core observation data, thin slice analysis, and image logging, the cave-fractured reservoir was primarily developed in the actic region near the side of a depositional fault. Tectonic and diagenetic fractures were the primary types of fractures. High-angle tectonic fractures in the closure and open status were developed well in dolomitic mudstone, while a low-angle fracture and reticulate fractures were developed in the tectonic-hydrothermal hybrid process and were filled with hydrothermal minerals. The reservoir was located in low-lying land; therefore, detrital grain pressolution fractures were formed by burial diagenesis. Intergranular and intragranular dissolved pores, which were formed by hydrothermal activity, were developed primarily in the highly dolomite lithology. According to the diagenesis temperature of dolomite from a carbon-oxygen isotope analysis, multiple hydrothermal fluid injection events occurred, and dolomitization ensued before massive hydrocarbon migration. The dissolution of organic acids formed by hydrocarbon charges after dolomitization and inorganic acid produced by burial diagenesis for soluble minerals effectively promoted the reservoir properties. Strong heterogeneity due to lithology and fracture-vug systems led to intricate oil-water relationships. Four statuses occurred, including cave-fracture oil, isolated oil, stored oil, isolated water, and stored water. The oil-water distribution patterns were established based on the core observation.

*Hydrothermal dolomite; fracture-vug reservoir; oil-water distribution; North China; Erlian Basin*

## 1. INTRODUCTION

Hydrothermal dolomite has recently been found in the Tarim Basin (Li et al., 2016; Zhu et al., 2015; Guo et al., 2016), the Jiuquan Basin (Fan et al., 2003; Wen et al., 2013), the Erlian Basin (Guo et al., 2013), the Sichun Basin (Liu et al., 2014; Liu et al., 2016; Feng et al., 2017) in China, the Northeast Basin (Diehl et al., 2010; Hendry et al., 2015; Slater and Smith, 2012) in the USA, and the West Basin (Qing and Mountjoy, 1994; Schrijver et al., 1996; Conliffe et al., 2010; Morrow, 2014) in Canada. There are many ways to study the genesis and recognition of structure-controlled hydrothermal dolomite (Al-Aasm, 2003; Debruyne et al., 2016; Hendry et al., 2015; Fan et al., 2003; Dai et al., 2004; Graham et al., 2006). Authors primarily focused on petrology characteristics, which were related to hydrothermal fluid, such as saddle shaped dolomite crystals, hydrothermal fluid mineral combinations of analcite-giobertite-siderite and the characteristics of carbon-oxygen isotopes. However, few studies examine the influence of cave-fractured reservoirs formed by hydrothermal on oil-water contact.

Evidence of oil in the dolomitic mudstone cave-fractured at well X26 was found in 2009, producing more evidence regarding fractured mudstone oil, and this finding was further confirmed by a mudstone cave-fractured hydrocarbon reservoir in Xilinhaolai area, Baiyinchagan sag with the successful drillings of wells X3-69 and X31. This area is now a significant oil exploration area. The latest research indicated that fractures and solution vugs could provide favorable reservoir space and flow pathway for petrology, solution promoted reservoir space and fracture linked up of different types that improved the connectivity and permeability. At the same time, fractures were the key factors for hydrocarbon accumulation and high levels of production. Therefore, understanding the distribution characteristic of fracture and dissolution vugs and their impact on oil-water distribution was very important for the hydrocarbon exploration and development of the Xilinhaolai area, Baiyinchagan sag.

Guo et al. (2012) and Hu et al. (2013) discussed the genesis, petrology characteristic, seismites, the origin of  $Mg^{2+}$  and the distribution of Lower Cretaceous structure hydrothermal dolomite in Baiyinchagan sag. Results suggested that dolomite formed under the condition of xerothermal and depositional fault connected supra-crustal hydrothermal fluid upwelling fluid dolomized marlstone on the hanging wall. Yue et al. (2009) studied the two special geological phenomena of deformation and chink and deemed that seismic and tectonic forces

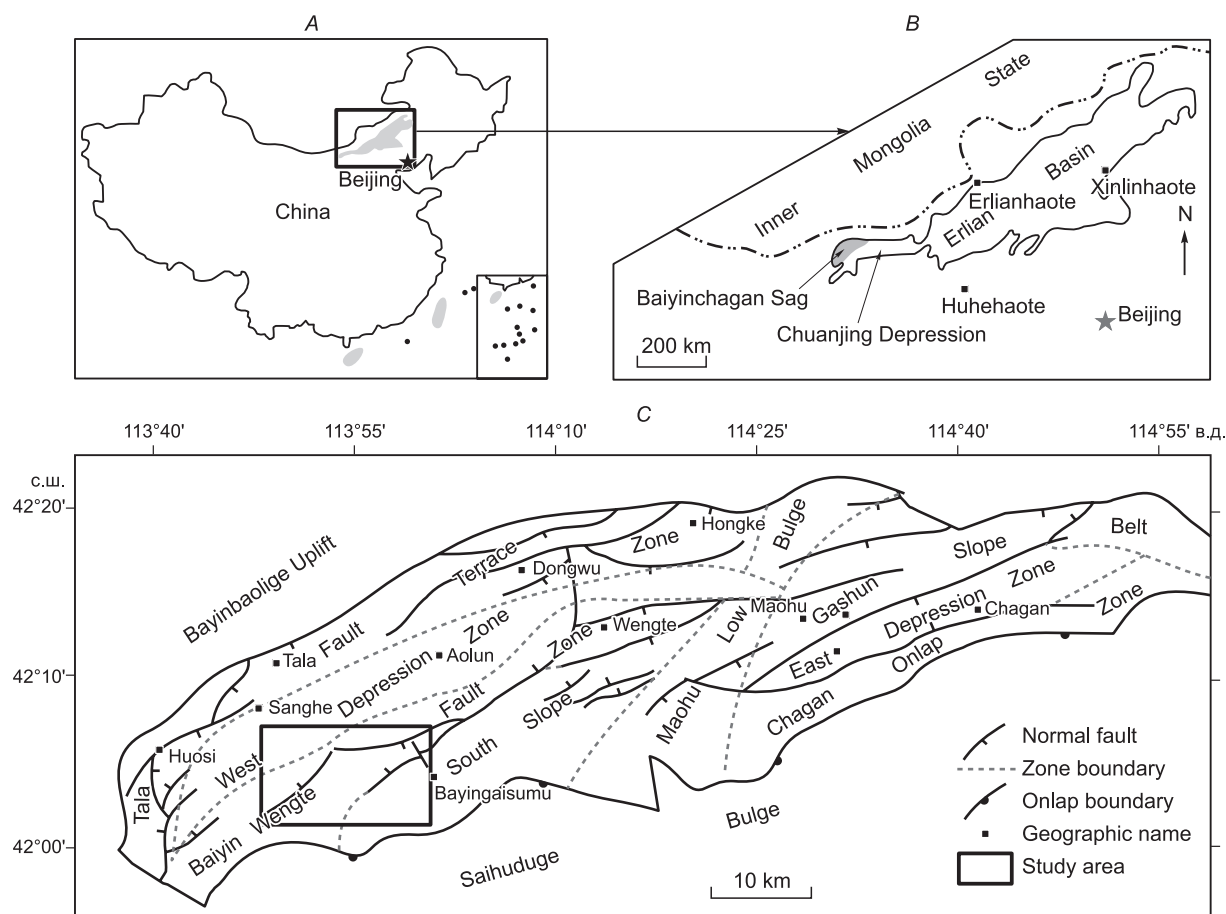


**Fig. 1. A, B, C are the structural locations of the Erlian Basin, the Baiyinchagan sag and the Xilinhaolai area, respectively (modified from Deng et al., 2013).**

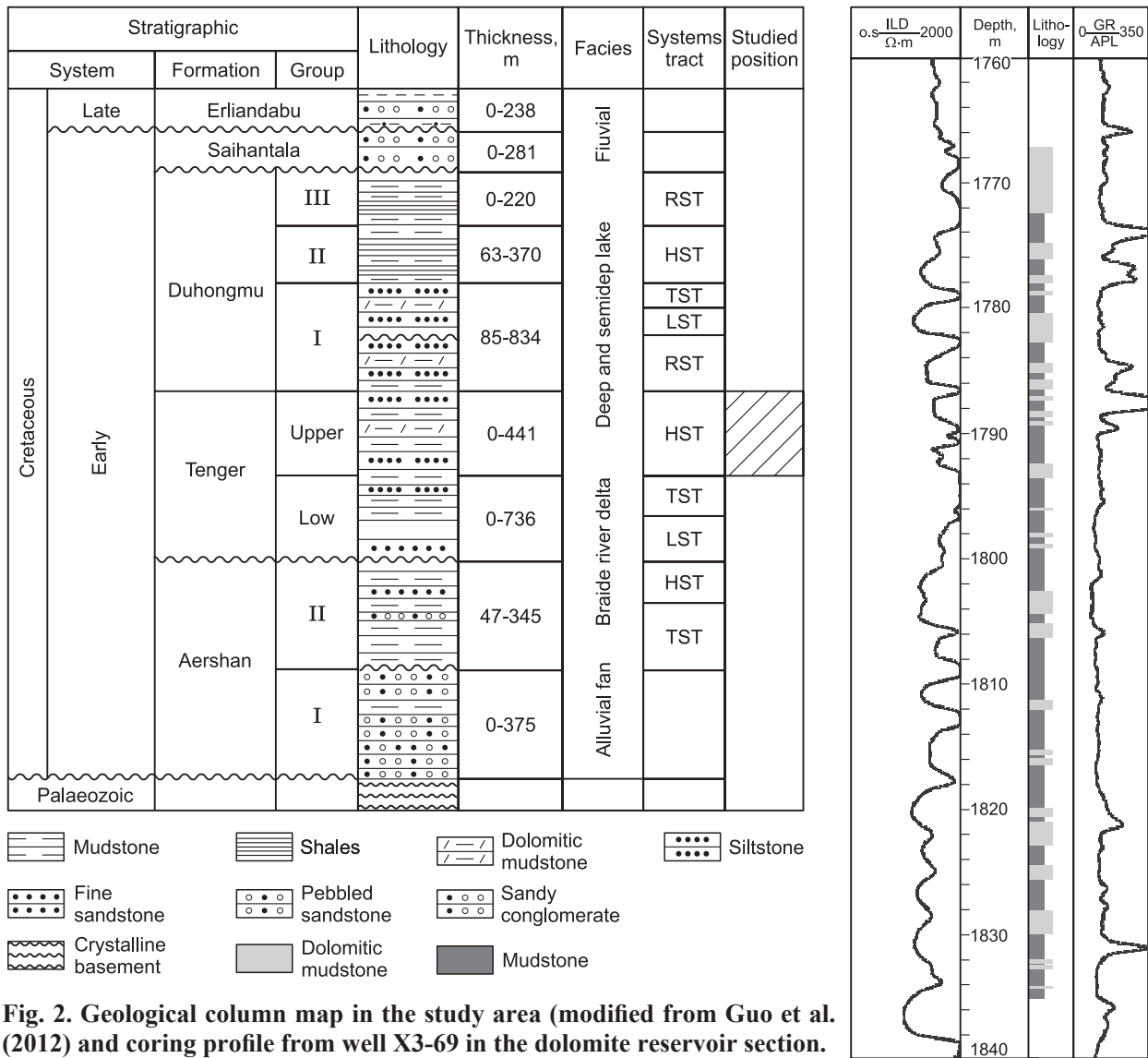


**Fig. 2. Geological column map in the study area (modified from Guo et al. (2012) and coring profile from well X3-69 in the dolomite reservoir section.**

were formed microfaults, crack networks and sandstone veins. However, this research did not include fracture characteristics.

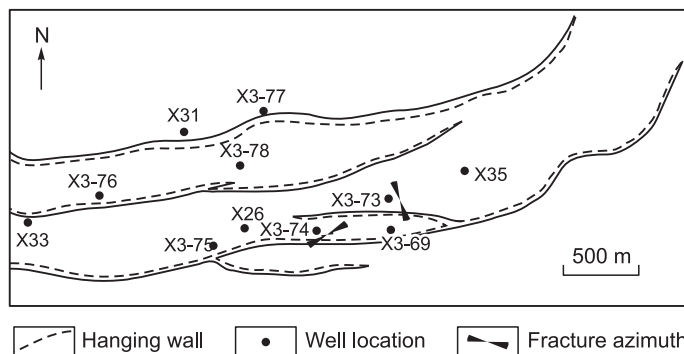
This paper used well logs imaging of 3 wells, nuclear magnetic resonance logs of 2 wells, cores observation data of 3 cores, 24 casting sheet slices and the common slice of one cored well, well testing data and cores petro-physical analysis data to discuss the fracture-vug characteristics and their influence on oil and water distribution.

## 2. GEOLOGICAL SETTING

Erlian Basin was located in the center of the Inner Mongolia autonomous region in North China and was a primary Mesozoic strata continental rifted basin developed on the Hercynian folding basemen (Fig. 1, A). Baiyinchagan sag was located in the west margin of the Erlian Basin and is a secondary tectonic unit of the north Chuanjing depression. This location was a dustpan-shaped faulted sag that faulted to the west and overlapped to the east (Fig. 1, B) (Huang et al., 2003; Zuo et al., 2016). The Xilinhaolai area included the sub-tectonic units in the Baiyinchagan sag and was located in the southern slope of the western areas, whose structure was a monocline striking NE, and dipping to the NW (Fig. 1, C).

The Cretaceous sequence can be divided into the following five formations: Aershan, Tenger, Duhongmu, Saihantala and Erliandabu Formations, proceeding from bottom to top (Fig. 2). The overall depositional stage of the Lower Cretaceous of Baiyinchagan sag was lacustrine transgression to regression (Zhang et al., 2005). The sediment of early Aershan Formation are alluvial fan system, and the sediment of late Aershan formation and lower part of Tenger Formation are a braided-river delta system. The sediment of the upper part of the Tenger and Duhongmu Formations are a deep lacustrine system. The main target bed was a Tenger Formation of low-

**Fig. 3. Relationship between structure distribution and fracture azimuth in the study area. Fracture azimuth data from imaging logs of well X3-73 and well X3-74.**



er cretaceous, which could be divided into two parts, the upper part was mainly mudstone and the lower part was interbedded sandstone and mudstone. The fracture-vug reservoir is in the lower part of upper Tenger Formation, which occurred in the subsag depression, with a thickness of 50–110 m, and the lithology are mainly dolomitic mudstone and argillaceous dolomite (Fig. 2).

### 3. DATA AND METHOD

The types of fractures and distribution features are determined based on imaging logs and cores observation. Nuclear magnetic resonance (NMR) is used to measure the difference and distribution of petrophysicals data by logging and analyzing the cores data. The carbon-oxygen stable isotope data were measured from the Jiangnan Oilfield, Sinopec, and it was used to calculate the temperature and saline of the dolomite that determined the dolomite diagenesis environment in the study area. Based on the thin section and fluid inclusion homogenization temperature that from the Zhongyuan Oilfield Company, Sinopec, the factors that controlled the development of fractures and vug are definite. The production data showed the influence of lithology and fracture-vug development regularity on production of that reservoir. Finally, the cores observation helped a model of the oil and water distribution in the study area to be developed.

Seven fresh rock samples of argillaceous dolomite and dolomite rock were crushed into 100–500 mg and dried at 60 °C for 12 hours later baked at 110°C for 3 hours. The oxygen and carbon isotope analyses were carried out with a MAT253 mass spectrometer at the Jiangnan Oilfield Company, Sinopec, using the standard methods described in Ebube et al. (2013) and the sample preparation method described in Karem et al. (2008). Tests on the dried dolomite powder samples (10–50 mg) selected from dolomite rocks and argillaceous dolomite were conducted in an inert atmosphere with ultrapure concentrated (100%) orthophosphoric acid, and CO<sub>2</sub> was collected after 72 hours of constant temperature reaction and analyzed on a MAT253 mass spectrometer.

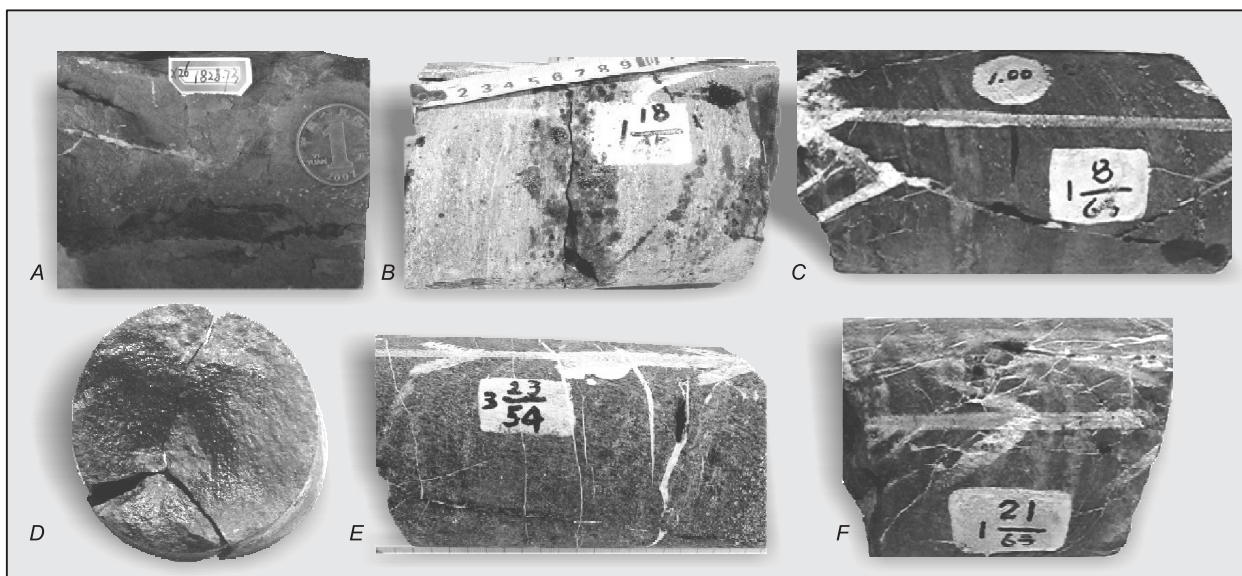


**Fig. 4. Characteristics of different types of fractures in the cores wells.**

A, Oil invaded into suture lines formed by pressure solution in well X26, dolomitic siltstone at 1828.73 m. B, Dissolution fractures connected caves of well X3-69, dolomitic mudstone at 1768.45 m. C, Oblique fractures were partly filled by calcite of well X31, argillaceous dolomite at 2012.23 m. D, Vertical fracture s with oil saturated bed of well X3-69, dolomitic mudstone at 1775.62 m. E, Low angle fractures were filled by calcite of well X31, dolomitic mudstone at 2032.73 m. F, Network fractures were filled by calcite in well X31, dolomitic mudstone at 2014.01 m.

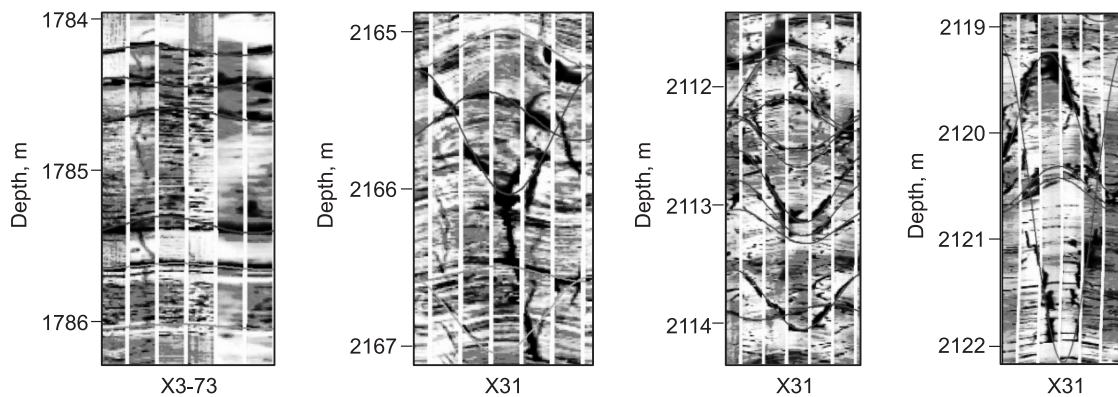


**Fig. 5. Characteristic of imaging logs with different dip-strikes. Green line is the bedding plane. Red line is the open fracture. Ice blue line is the induced fracture.**

The isotope data are reported in the  $\delta$ -notation relative to the PDB standard, and each of the samples was tested at least twice to ensure that the difference between the two measured values was within 0.2‰, and the data reported in this paper are the average of the two measured values.

## 4. RESULTS

### 4.1. Types and characteristics of fractures

Fractures in the study area were divided into tectonic fractures and hydrothermal fractures formed in hydrothermal diagenesis. Tectonic fractures developed well in the fracture reservoir and expanded further with various fillings. The oblique fractures and high angle fractures were the main types. According to interpretation data of the imaging logs, the fracture azimuths were consistent with structural data (Fig. 3), and favorable fracture cellular systems formed between fractures. The sutures formed by dolomite and argillaceous dolomite are the main types of diagenetic fractures (Fig. 4, A). Dissolution fractures usually accompanied corrosion as a communication bridge for solitude caves (Fig. 4, B), which were secondary fractures formed by underground hydrothermals migrated along the fault and dissolved in the host rock. Therefore, dissolution fractures mainly distributed near the discordogenic fault.

Fractures could be divided into oblique fractures, low angle fractures, network fractures and high angle fractures according to the fracture attitude. Oblique fractures and high angle fractures were the main types, and the former typically appeared with a number of shear fractures that cut each other (Fig. 4, C). The imaging log demonstrated a low curvature of the sine curve that crossed over other fractures (Fig. 5, A). The larger fracture aperture sections were usually filled with calcite or gypsum and were smaller than 1.5 mm (Fig. 4, C). High angle fractures usually developed near faults with a large aperture in oil invasion, and the fracture plane was smooth (Fig. 4, D). The imaging log demonstrated a high curvature sine curve crossing over the other fractures

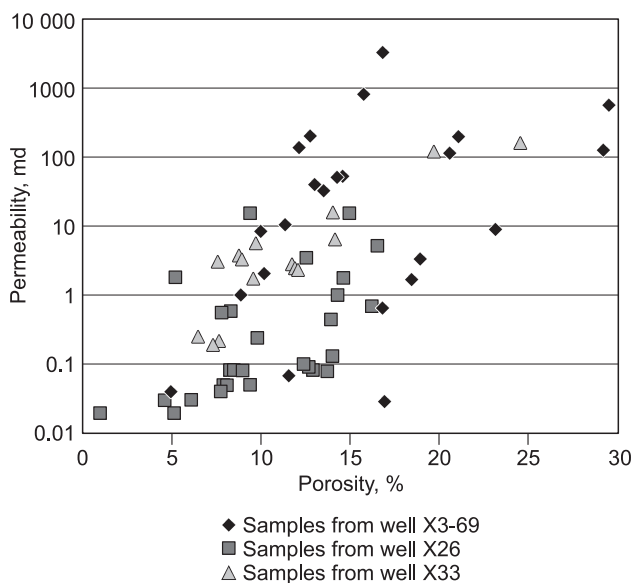


(Fig. 5, B). The horizontal range of low angle fractures were short (typically shorter than 15 cm), and most fractures were filled in a shape of a fusoid that was larger in the middle and smaller on the two sides with a parallel distribution as hairline (Fig. 4, E). The imaging log demonstrated a low amplitude fluctuate in the situation that paralleled the other fractures (Fig. 5, C). Network fractures were assemblage of multiple sets of high angles and oblique fractures; they crossed over each other and formed net-like crossing fractures (Fig. 4, F), whose imaging logs were shown as deep red sine curves crossing over each other (Fig. 5, D).

**Fig. 6. Relationship between permeability and porosity from 51 cores sample analyses and NMR interpretation in the dolomite reservoir. There are 23 cores in well X3-69 and 28 cores in well X26.**

## 4.2. Fracture-vug reservoirs characteristics

### 4.2.1. Petrophysicals of fracture-vug reservoirs

The petrophysical property data of the dolomitic reservoir were from 2 cored wells and a well of NMR interpretation. Cores analysis were obtained by kerosene saturation method using a rod shaped of the cores with that was 25 mm × 50 mm. The survey mode of D9TW and D9TE312 was taken in well X33 of NMR, and the petrophysical porosity and permeability data obtained from difference spectrometry analyses were used. The porosity of the dolomitic reservoir ranged from 1% to 29%, with an average of 12.1%, and the permeability were mostly lower than 100 md, with an average of 86.4 md. Many fractures and vug occurred, so the porosity and permeability values varied (Fig. 6).

Secondary pores were the main reservoir space, which included the intergranular and intragranular dissolution pores, the moldic pore, and the dissolution fracture that produced by organic and inorganic acid from the hydrothermal fluids and hydrocarbons.

The secondary dissolution cavity was the key to promote reservoir porosity. Fractures were important reservoir space and connected the solitude cavity, which made it important to improve permeability. The permeability of a sample without fractures was lower than 10 md, while the porosity of other samples with a composite of the dissolution cavity and fracture could reach 29.5%, and permeability could reach 1000 md (Fig. 6).

### 4.2.2 Fracture-vug reservoirs parameters

Two prominent peaks in fracture intensity occurred ranging from 1.5 to 2 items per meter and 3 to 5 items per meter, and the former was priority with an average of 2 items per meter. Most lengths were 2 to 2.5 m/m<sup>2</sup>, with an average of 2.4 m/m<sup>2</sup>. The hydrodynamic fracture width was from 10 to 30 μm, with an average of 27 μm (Fig. 7). Compared to cores observation (Fig. 4), the width was obviously smaller because fractures are

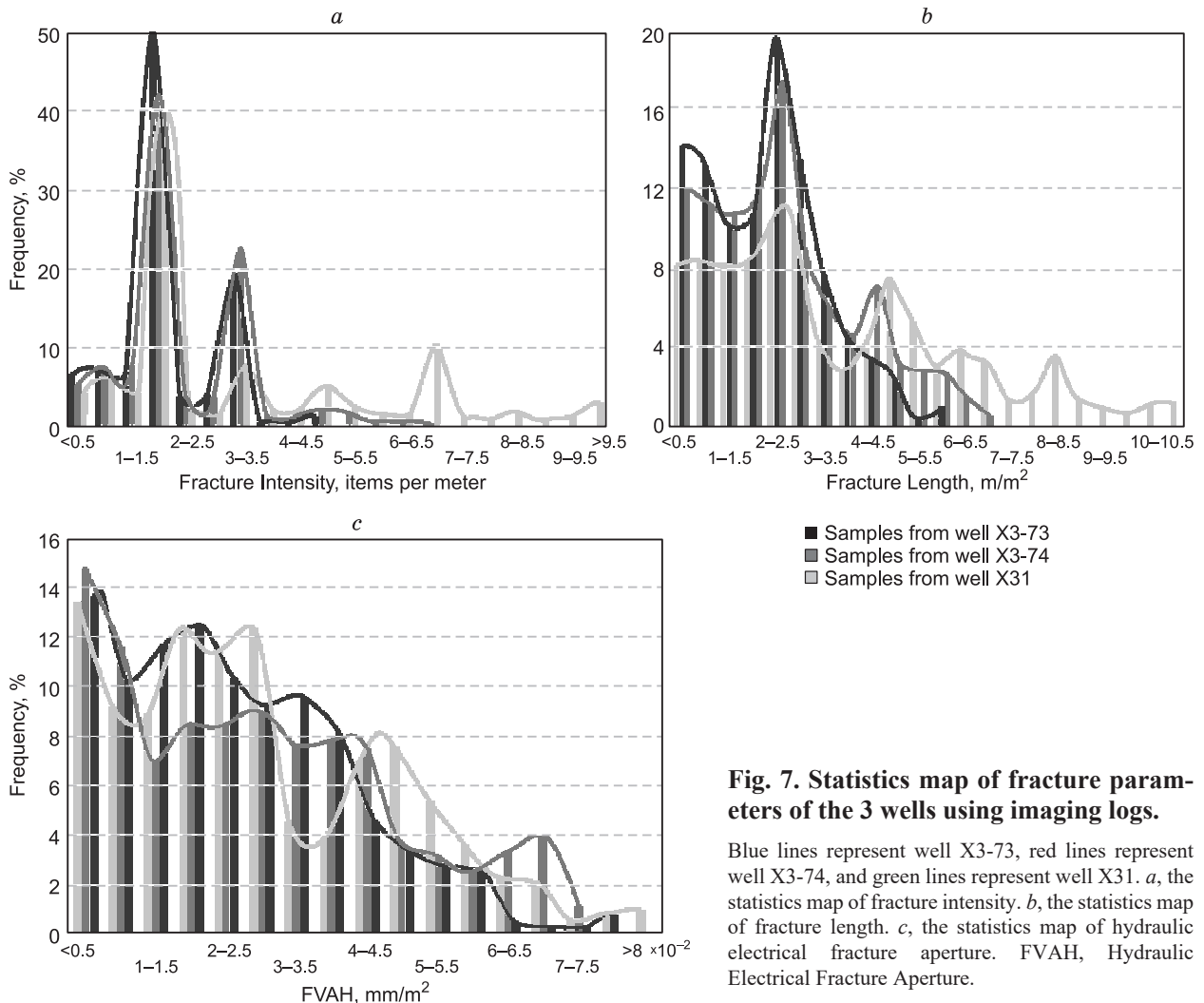


**Fig. 7. Statistics map of fracture parameters of the 3 wells using imaging logs.**

Blue lines represent well X3-73, red lines represent well X3-74, and green lines represent well X31. *a*, the statistics map of fracture intensity. *b*, the statistics map of fracture length. *c*, the statistics map of hydraulic electrical fracture aperture. FVAH, Hydraulic Electrical Fracture Aperture.

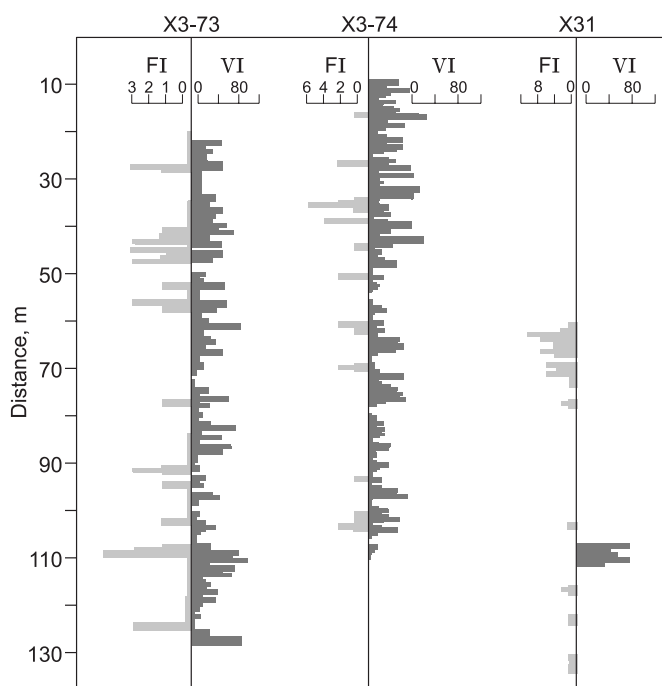


**Fig. 8. Fracture intensity and longitudinal distribution.**

Distance was away from the top bed of fracture and vug reservoir in the dolomite reservoirs. FI was the fracture density of the opening fracture, items per meter. VI was unfilled vug density, numbers per meter. The well locations can be seen in Fig. 3.

sensitive to stress (Smart et al., 2001; Zeng et al., 2007c). The fracture growth sensitivity and the fracture scale growth and permeability (Zeng, 2010) resulted in fracture porosity and permeability that were larger on the surface than in formation conditions.

There was no meaning to the statistics the fracture parameters and cavities in well X31 because the cavity was undeveloped (Fig. 8). The fracture and cavity areas were primarily from 200 to 1550 mm<sup>2</sup>, and the average was 1151 mm<sup>2</sup>. The plane porosity ranged from 5% to 10% and was less than 5%, with an average of 11%. Density was mainly from 5 to 60 per meter (Fig. 9), and

the average was 31. The distribution of the fracture-vug in the vertical direction clearly showed segmentation (Fig. 8), which may be concerned with hydrothermal fluid filling in the pulse.

### 4.3. Fracture-vug reservoirs control parameters

#### 4.3.1. Relationship between dolomitization and oil charging

The data of stable isotopic is useful in determining the diagenesis environment of dolomite. The data of  $\delta^{13}\text{C}$  can be used to measure the diagenesis salinity. High diagenesis temperatures result in oxygen isotopes migrating to negative values, and carbon isotopes were heavier in the closed environment than in the open environment, while carbon isotopes were lighter after the leaching of atmospheric water and hydrocarbon fluid denudation (Hardie, 1987; Allan and Wiggins, 1993).

Keith and Weber (1963) proposed a formula to calculate the palaeosalinity using  $\delta^{18}\text{O}$  and  $\delta^{13}\text{C}$ , which is  $Z = 2.048 \times (\delta^{13}\text{C} + 50) + 0.498 \times (\delta^{18}\text{O} + 50)$ . Where Z was larger than 120, indicating marine facies, otherwise indicating lacustrine facies. According to the interpretation results of the C–O isotope (Table 1), the Z values of all samples were larger than 120 and were against sedimentary setting. However, a high salinity result may be relevant to the hot hydrothermal brine, which was brought about by supracrustal tectonic activity rather marine facies causes the high salinity.

The temperature of dolomitic diagenesis calculation adopted the formulation established by Epstein (1963) and was  $T = 14.8 - 5.4 \times \delta^{18}\text{O}$ . The results were shown in Table 1. Two cycles in temperature from the result of well X3-69 are shown in the columns, which were from high temperature to low, and the reverse circle is shown from bottom to top (Table 1). The cycle change of the hydrothermal fluid from sedex to effluent and then to sedex was indicated by the results.

Table 1. Carbon oxygen isotope data and its interpretation

Well	Sample depth (m)	Lithology	$\delta^{13}\text{C}_{\text{PDB}}$	$\delta^{18}\text{O}_{\text{PDB}}$	Diagenesis temperature °C	Z
			‰			
X3-69	1697.2	Dolomite	4.9	-15.9	100.66	129.4
X3-69	1770.6	Dolomite	3.9	-14.7	94.18	127.9
X3-69	1773.8	Dolomite	3.3	-12.4	81.76	127.8
X3-69	1775.2	Dolomite	3.3	-14.4	92.56	126.9
X3-69	1778	Argillaceous dolomite	4.3	-15.5	98.5	128.4
X3-69	1815.39	Argillaceous dolomite	3.7	-15.9	100.66	126.9
X26	1821.15	Argillaceous dolomite	3	-8.2	59.08	129.4

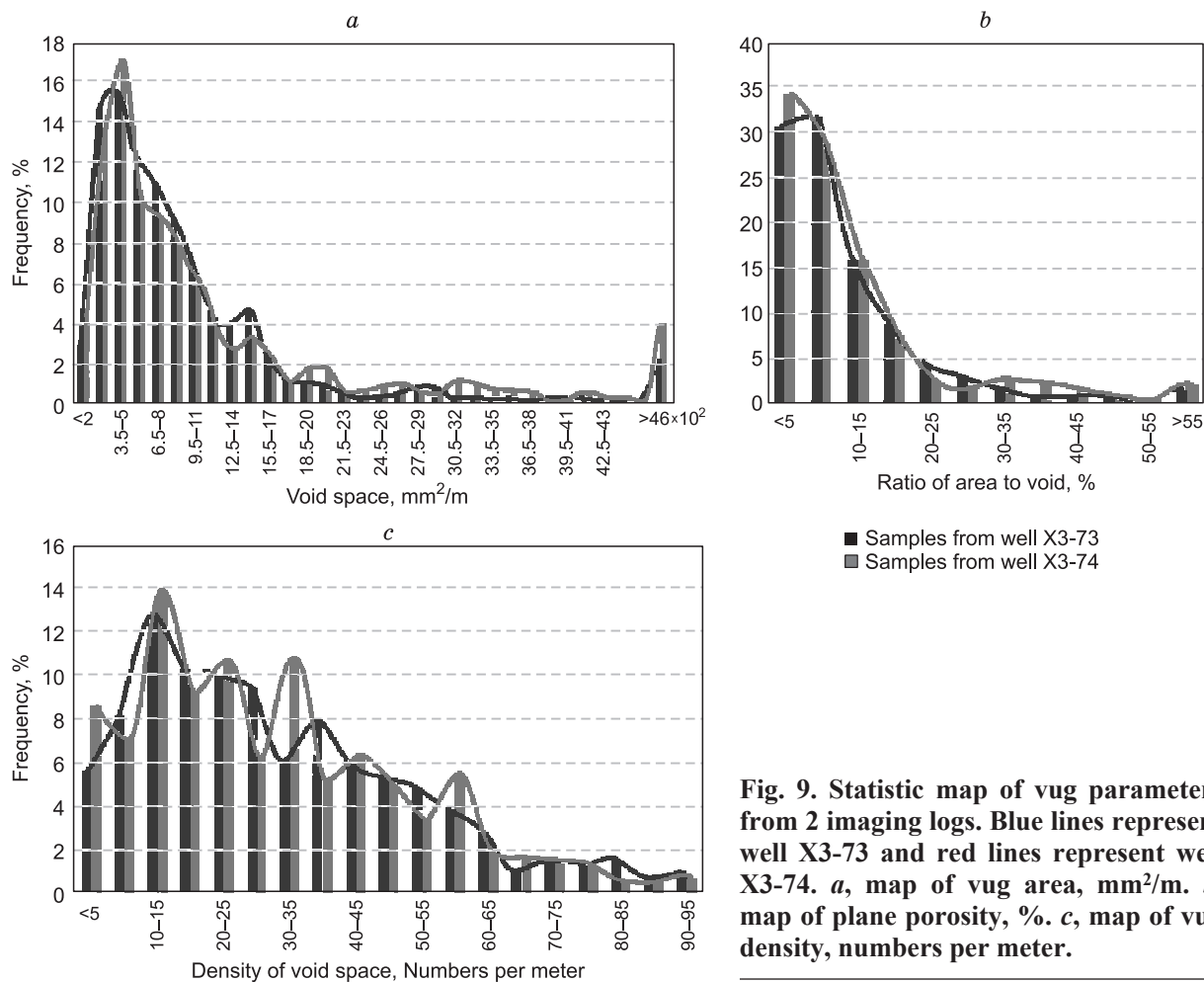


**Fig. 9. Statistic map of vug parameters from 2 imaging logs. Blue lines represent well X3-73 and red lines represent well X3-74. a, map of vug area, mm<sup>2</sup>/m. b, map of plane porosity, %. c, map of vug density, numbers per meter.**

The data of  $\delta^{18}\text{O}$  was from  $-8\%$  to  $-16\%$  (Fig. 10), the average was  $-13.8\%$ , and the main reason for extremely negative results was because the oxygen isotopic was distilled by hydrothermal fluid. The distribution of  $\delta^{13}\text{C}$  was from  $3\%$  to  $5\%$ , the average was  $3.8\%$ , and the heavier carbon isotopes indicated that dolomite formed in the condition of inorganic carbon. Hence, hydrothermal dolomite was formed before extensive hydrocarbon migration.

#### 4.3.2. Controlling of the structural and hydrothermal properties

Faults are three-dimensional geologic bodies with a complex architecture (Caine, 1996; Gudmundsson et al., 2001; Aydin, 2000; Yielding et al., 2000). In bilateral areas confined by faults and the ending fault sections, where stress was released, were the major zones of induced fractures that could form complex fracture systems. Although vugs undeveloped in well X31 (Fig. 8), a complex network and high angle fractures also developed due to close proximity to the faults (Fig. 3). Due to lack of hydrothermal minerals to fill, new fractures could be formed by acid dissolution in the later stage while retaining the initial fracture. Therefore, the parameters of tectonic fractures typically have large values.

The hydrothermal fluid in the basin increased from deep strata to shallow beds along the fault and was hotter as well as more salty and acidic than in the upper beds (Hanor, 1994; Heydari, 1997). The hydrothermal fluids and organic acids in the later stage migrating to the upper direction along existing fractures dissolved them, which expand the existing fractures further and formed corrosion fractures and vugs systems. The oil charging in the later stage also made fractures corrode even further.

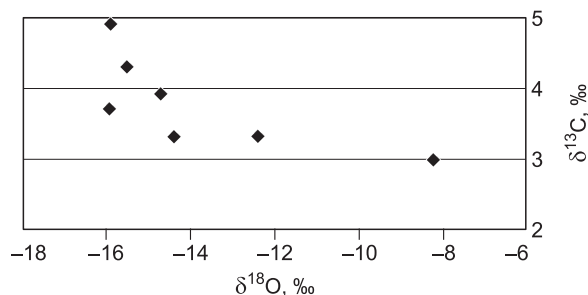


**Fig. 10. Crossplot of  $\delta^{13}\text{C}$  to  $\delta^{18}\text{O}$  of dolomite in the third formation of the upper Tenger Formation.**

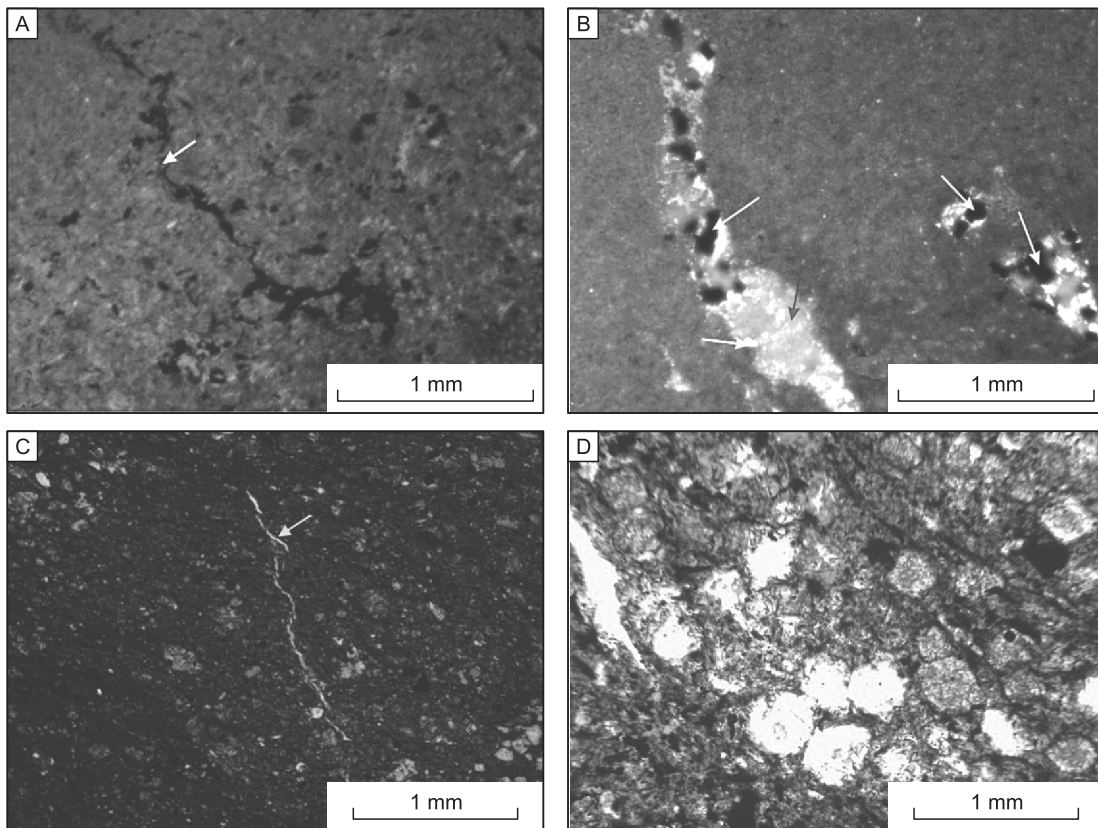


**Fig. 11. A, Microfractures and dissolution vugs in well X26 (1826.8 m), orthogonal polarization 25 times, dolomitic mudstone, microfractures were fully filled by argillaceous (yellow arrow) and hydrocarbon (red arrow), orthogonal polarization; B, dolomitic mudstone in well X26 (1816.03 m), orthogonal polarization 25 times, dolomitic mudstone, dissolution fracture and vug were partially filled by siliceous (ice blue arrow), lime (green arrow) and pyrite (yellow arrow); C, argillaceous mudstone in well X3-69 (1805.67 m), plane-polarized light 25 times, microfractures were filled by zeolite and develop zeolite solution pores; D, dolomitic mudstone with oil intrude in well X3-69 (1766 m), plane-polarized light 25 times, oil soaked dolomitic mudstone, analcite solution pores.**

Although hydrothermal fluid dissolution fractures and vugs may be partially (Fig. 11, A, B) or even fully filled (Fig. 11, C) by hydrothermal minerals in later stages, these fractures and vugs are pathways of hydrothermal migration, which are the main reason that dissolution vugs are commonly associated with fractures (Fig. 11, C). The hydrothermal precipitation minerals in the early stages can be dissolved to form solution pores (Fig. 11, D) by organic and inorganic acids. Additionally, the hydrothermal migration pathways formed corrosion weak zones, which are the advantageous pathways for oil migration. The overlying thick mudstone was a good cap rock and is a good lateral occlusions bed in the offside, which is advantageous for oil and gas accumulation in fracture-vug reservoirs. At the same time, organic acids from hydrocarbons could dissolve partial fillings minerals (mainly zeolite) in early hydrothermal fractures and improve the petrophysical properties of the reservoir.

The Tenger Formation was created during strong depression. The active hanging wall held most of the strain, and fractures developed because the extensional fault activated strongly. Later, hydrothermals surged into the reservoir under the fault activity episode. Unsaturated hydrothermals migrated along the faults and fractures and passed into the reservoir and dolomized host rock to enlarge fractures and transform them into dissolving fractures. While in the process of dolomitization, however, various hydrothermal minerals (e.g., anhydrite, analcinite, pyrite, and quartz) achieved saturation and evolved by incipient crystallization due to decreased temperature. This process could replace host rock, resulting in gypsification in a wide area and causing damage to original fractures and pores (Fig. 12). Therefore, hydrothermal in the early stages could broaden present fractures and damage fractures by minerals precipitating in later stages. Some researchers (Hu et al., 2013) have suggested that gypse in the Tenger Formation formed under the condition of drought and evaporation. However, marker sediments were not found in well cores from the same layer in the slope zone in that

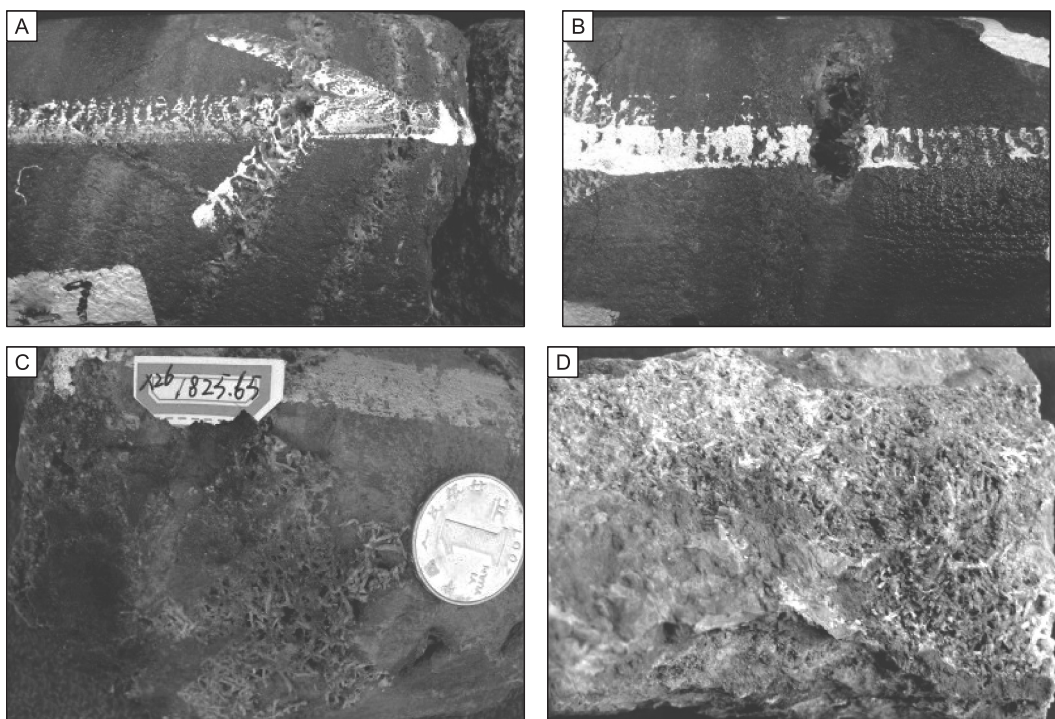


**Fig. 12.** A, dolomitic mudstone of well X3-69 at 1804.6 m, fractures were filled by gypse. B, dolomitic mudstone by oil cut of well X3-69 at 1804.9 m, fracture and dissolved vug were partially filled by gypse. C, dolomitic siltstone by oil cut of well X26 at 1825.6 m, fracture were filled by gypse and dissolved pore in gypse. D, dolomitic siltstone of well X26 at 1827.6 m, fracture were fully filled by gypse.

environment. It is likely that the gypse in the depression was supersaline hydrothermal brine dolomized host rock and precipitated when the temperature decreased.

The hydrothermal fluid took a long time to be detained in the horizontal and low dip fractures, which caused hard saturated hydrothermal fluid movement. Although fractures opened in the early stage, various minerals related to hydrothermal fluid precipitated in later stages and resulted in some fractures being fully or partially filled by hydrothermal minerals. For high dip angle fractures, under the function of seismic pumping in early stage, hydrothermal fluid went up along the extensional faults, and the associated fractures flew upward. At the same time, the high dip angle fractures were beneficial to continuous unsaturated and saturated hydrothermal fluid diagenetic fluid exchange. Fractures could be reconstructed and the surrounding rock could be corroded to form solution pores. The cold hydrothermal fluid in later stages caused the fluid density to increase. Saturated fluid flew back downstream under gravitation function, so mineral precipitation in the downward direction was enhanced and fracture aperture decreased. Due to organic acid dissolution and cooling effect, the dissolving vugs superposed development along the former cave-fractured zones in an upward direction and could alter the former microfractures into dissolving fractures with a larger aperture. So, fractures with large dip angle usually were called open fractures, whose upward direction fractures were seldom filled by hydrothermal minerals.

#### 4.3.3. Controlling burial dissolution

The dolomite reservoirs were in the later stage of diagenesis (Xu et al., 2005), and the Tenger Formation itself had hydrocarbon generation potential and a hydrocarbon generation peak during the Duhongmu formation sedimentary period (Liu and Zhang, 2011). Organic acid was generated from numerous matured

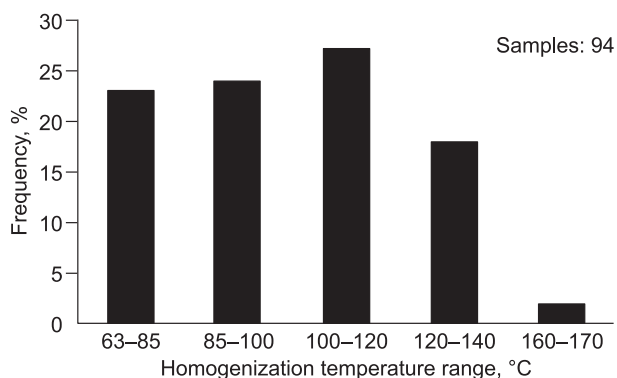


**Fig. 13.** Histogram of homogenization temperature from fluid inclusion in the Tenger Formation.

hydrocarbons, which dissolved partially soluble materials and microfractures generated from early fault activities and hydrothermal brine and formed dissolving fractures and vugs. Hydrocarbons could initiate thermochemistry sulfate reduction (TSR) with sulfate (i.e., gypse) when fluid temperatures were higher than 120 °C, which could generate alternative hydrocarbons, fix bitumen, CO<sub>2</sub> and H<sub>2</sub>S as well release heat. Inorganic acid was generated when H<sub>2</sub>S and CO<sub>2</sub> were dissolved in water, which was a significant agent for carbonatite burial dissolution (Mazzullo, 1981, Mazzullo and Harris, 1992). The distribution of homogenization temperature data (Fig. 13), which was obtained from 94 dataset, indicated that multi-phase of hydrocarbon charging, and when the temperature was higher than 120 °C, asphalt of blocked fractures (Fig. 11, A) could be the possible product

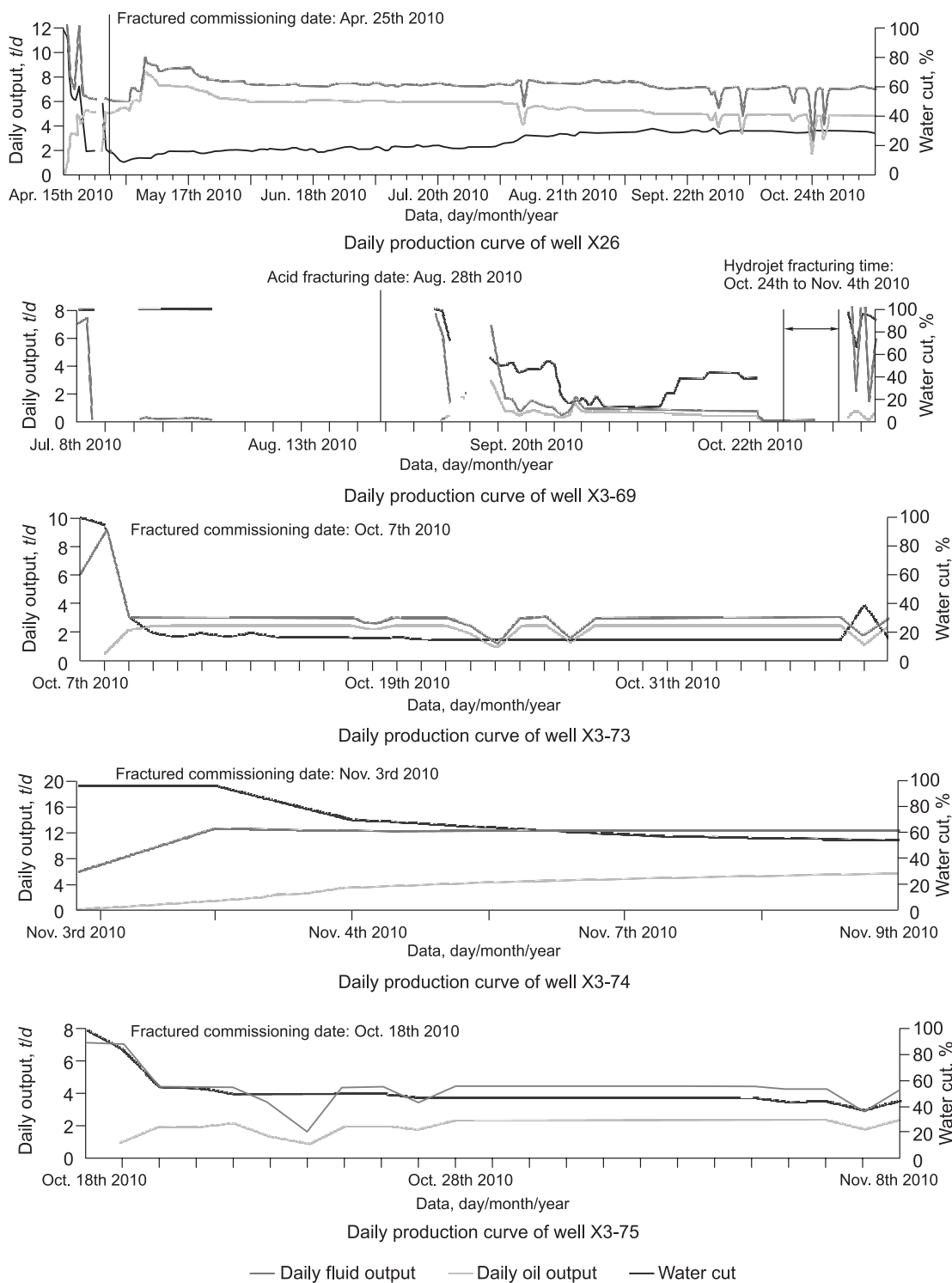


**Fig. 14. Production history curve of typical wells in the dolomitic fracture-vug reservoir.**

of hydrocarbons, and sulfate mineral alteration hydrocarbon fluid existed in the Tenger formation. Inorganic acid generated from alteration could enhance the dissolution of the soluble minerals of zeolite and calcite.

#### 4.4. Production history characteristics and the oil-water distribution model

##### 4.4.1. Production history

Dolomitization inhomogeneity resulted in a large difference in the dissolution of hydrothermal fluid, organic and inorganic acid to dolomite, and strong heterogeneity in the reservoir. There was no output change in the conventional opening, and the fracturing effect was widely different between the different wells (Fig. 14). The X26 well production for a period of time and productivity was stable after fracturing, and the oil production remained constant at 5 tons per day. The X26 well was located on the downthrown side of the syngenetic sedimentary faults. Siltstone of the upthrown block was injected into the downthrow as gravity flow, so shale content was less. Dolomitic siltstone and silty dolomite were the primarily types of reservoir and was beneficial for fracturing. At the same time, the sand caused the pressure cracks to form stable products. There was a good match between the fracture intensity and vug location in the X3-73 well and the X3-74 well (Fig. 8), and the production of both wells was stable. The fracture intensity of well X3-74 developed better than well X3-73, and therefore more fracture intersection with vugs occurred in the unit length, which enriched the seepage area in well X3-74. The production of well X3-74 was twice that of well X3-73; although, fractures developed in well X31, with no effective pores and vugs connected. The result was that no oil production occurred in the first conventional and second fracturing tests. There was no output in the early stage of well X3-69 in the dolomite reservoir. Daily oil production was 0.8 tons after acid fracturing and was 0.3 tons per day after hydraulic fracturing.

The X3-74, X3-75, X26 and X3-69 wells were located on the downthrown side controlled by contemporaneous faults. Only well X3-69 produced no oil through acid fracturing. The primary reason was that the well was located in the common downthrown side of contemporaneous and transform faults. They were both in the deep depression condition and lead to less sand deposits in the reservoir, which was hard to fracture, could not effectively support hydraulic fracture and was suitable to high production through acid fracturing. The sandy sedimentation of the delta front could be moved forward to the basin direction along the position of the transform zone (Gawthorpe and Leeder, 2000; Contreras and Scholz, 2001; Schelische, 1991; Scholz and Hutchinson, 2000) on the sides of wells X3-73, X35 and of X3-74, X26, X3-75. In this case, the wells could keep high oil production; for example, the production of X35 was up to 10.2 m<sup>3</sup> per day in the second fracturing oil test.

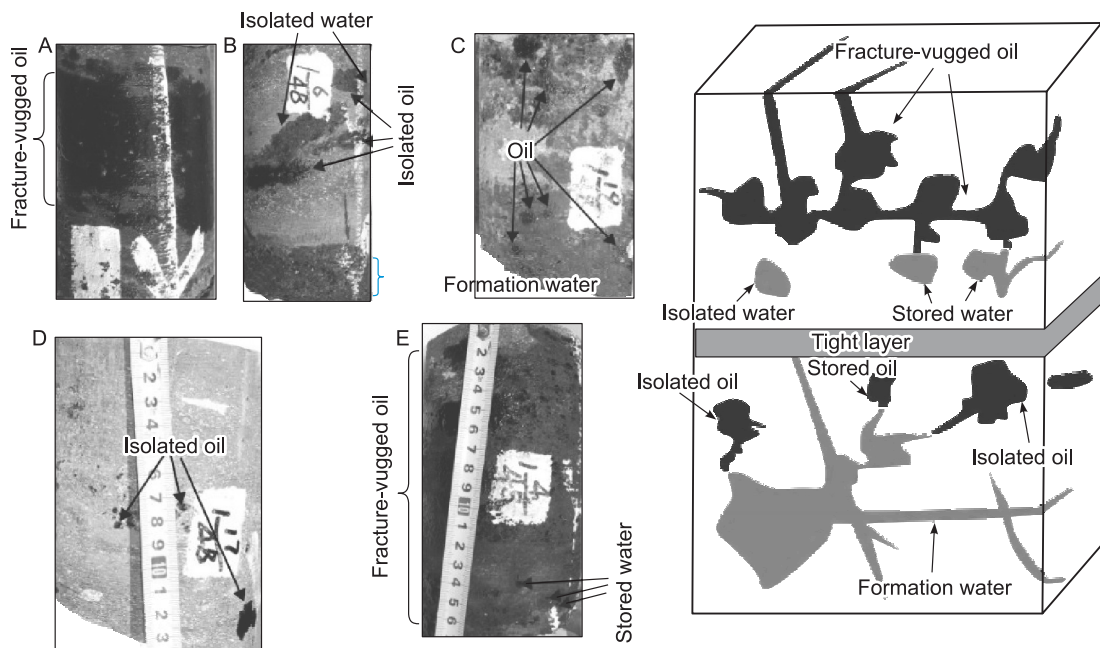


**Fig. 15. Model of oil-water distribution in dolomitic reservoir.**

A, the X3-69 well was at 1768.8 m, dolomitic mudstone, oil saturated in cave-fractured. B, the X3-69 well was at 1768.5 m, argillaceous dolomite, the fluid in bottom section was formation water and the upper section were isolated water and isolated oil, pay attention to the enrichment of pyrite at the water and oil contact. C, the X3-69 well was at 1772.2 m, dolomitic mudstone, oil spot scattered in formation water. D, the X3-69 well was at 1768.1 m, dolomitic mudstone, the bottom section was water and the upper section is oil.

#### 4.4.2. Oil-water distribution model

Reservoir space and pore structure between cave-fractured and the clastic reservoir was highly different, which resulted in reservoirs fluids with typical occurrence shape and division into isolated oil, stored oil, isolated water and stored water based on cores observation (Fig. 15). Stored oil means isolated dissolution pore space was charged by early oil migration. With organic acid dissolution and burial dissolution, the isolated oil contact with underlying formation water was fractured to form a united porosity-permeability system. Isolated oil was oil in isolated (Fig. 15, D, E) cavern oil accumulated in the early stage (Fig. 15, B) or isolated oil holes. Fractures contacted with formation water were filled by bitumen in later stages and hydrothermal minerals precipitation (i.e., pyrite, gypsum), which cut the connection of cave-fractured oil with basal water and it transformed the cave-fractured oil into isolated status. Isolated water was formation water that could not be replaced by hydrocarbons due to the lack of oil migrating pathways. Stored water was formation water located in the bottom of the reservoir and connected with the reservoir that was not totally replaced by hydrocarbons in the process of hydrocarbon replacing the formation water (Fig. 15, E). The fracture and vug development degree and their coupling relationship played a major role in controlling the oil-water distribution. The good connection of fracture and vug lead to strong regularity in fluid distribution; however, fractures and vugs with high intensity and bad connections lead to complex fluid distribution.

### 5. DISCUSSION

The dolomite vug-fractured reservoir was a rarely a “white smoke type” of nonmarine facies formed by hydrothermal sedimentary dissolution (Guo et al. 2013). The reservoir was linearly distributed along the discordogenic fault as the hydrothermal fluid pathway, whose fractures and vugs developmental degree was correlated closely with the fault. This paper only used image logging and cores observation data to analyze the longitudinally fracture and vug distribution, and its plane rules need further study to guide hydrocarbon exploration and development in the study area.

The diagenesis temperature of dolomite could not reflect the diagenesis temperature varieties of the whole dolomite interval; however, certain differences exist at certain intervals. If the hydrothermal fluid charged stage can be determined, it could better predicate lithofacies changes and longitudinal vug-fractured reservoir evolution regularity.

The fractures and vugs developed well in the dolomite reservoirs; tectonic fractures were the main developments, and high angle fractures were the main effective fractures. The development of tectonic fractures and vug dissolution were controlled by tectonics and lithology, although well X3-69 had a long massive oil saturated cores (Fig. 15, A) with high shale content and strong plastic properties. Acid fracturing was difficult, and low well productivity was the result. In contrast, the fractures and vugs were undeveloped in well X26, but with high sand content, fracturing was easy. The match degree between fractures and vugs had a great influence on production. The fracture intensity in well X31 was greater than that of well X3-73 and well X43-74, but a bad match occurred between fractures and pore dissolution in well X31; there was no productivity and no oil production in the continuous oil tests.

A difference in the vertical and horizontal hydrothermal dolomitization occurred and resulted in a great diversity in lithology and fracture-vug development regular patterns, which caused hydrocarbon selective charging. Under the burial influence in later stages, fractures played a role in connecting oil and water in the united reservoir system and were filled by hydrocarbon oxidized or hydrothermal minerals and split the united reservoir. This split led to complex oil-water contact, strong heterogeneity and various scatter oil spots in the formation water (Fig. 15, C).

This reservoir heterogeneity performed in the fracture-vug development, fractures-vug couple relationship and reservoir lithology. If lithology was stable, pore configurations were consistent with fracture and dissolved pores, and the reservoir would have better homogeneity and regularity of oil-water distribution. In contrast, if there was a great diversity in lithology, then anisotropics caused by lithofacies was strong. Additionally, dissolution fractures and pores had different development regularity because of different lithology, resulting in stronger heterogeneity and irregular oil-water distribution. As a result, launching high resolution lithology inversion was significant for reservoir development.

### 6. CONCLUSIONS

The fractures and dissolve pores were the main hydrothermal dolomitic reservoir space, and effective fractures were mainly high angle tectonic fractures, while low angle fractures were mostly filled by hydrothermal minerals in the study area.

Hydrothermal episodic charges were caused by fault episodic activity, which resulted in cyclicity in the dolomite diagenetic temperature. These results were different from dolomite formation that changed with vary-

ing hydrothermals at varying temperatures. As a result, there was a great variety in dolomite content in the longitudinal direction. It caused the development of fractures and vugs with segmentation in the columns. Dolomite was formed before the massive hydrocarbon migration in the study area; thus, organic acid formed in the later stages of hydrocarbon charging can improve the reservoir quality.

The upper dip direction of high angle fractures are usually opened due to the hydrothermal fluid dissolution and were typically effective fractures. However, low angle fractures were typically ineffective for hard to form continuous flowing alterations and were filled by saturated minerals after hydrothermal cooled and blocked the fractures.

Sand content is the key factor for controlling the output of dolomite reservoirs, and the high sand content is consistent with high yield. Lithology, the fracture and vug intensity and the coupled relationship control the distribution of oil and water. Strong heterogeneity and the specialty of the reservoir space resulted in the complex distribution of oil and water, including isolated oil, stored oil, isolated water and stored water.

### Acknowledgements

The authors are thankful for permission to published this paper and acknowledged for data contribution and sample collection from Zhongyuan Oilfield Company, Sinopec. We are grateful to anonymous reviewers for very constructive and useful comments.

### REFERENCES

- Al-Aasm, I.**, 2003. Origin and characterization of hydrothermal dolomite in the Western Canada Sedimentary Basin. *J. Geochem. Explor.* 78–79, 9–15.
- Caine, J.S.**, 1996. Fault zone architecture and permeability structure. *Geology* 24 (11), 1025–1028.
- Chi, Y.L., Zhang, W.X., Li, W.L., Dang, W.L.**, 1997. Evaluation of the prospective targets in the Baiyinchagan sub-basin (in Chinese with English abstract). *Fault-Block Oil and Gas Field* 4 (6), 5–9.
- Contreras, J., Scholz, C.H.**, 2001. Evolution of stratigraphic sequences in multisegmented continental rift basins: comparison of computer models with the basins of the East African rift system. *AAPG Bull.* 85 (9), 1565–1581.
- Conliffe, J., Azmy, K., Gleeson, S.A., Lavoie, D.**, 2010. Fluids associated with hydrothermal dolomitization in St. George Group, western Newfoundland, Canada. *Geofluids* 10 (3), 422–437.
- Dai, B.Z., Zhao, K.D., Jiang, S.Y.**, 2004. Modern sea-floor hydrothermal activity and genesis of massive sulfide deposites: An overview [in Chinese with English abstract]. *Bull. Mineral. Geochem.* 23 (6), 23–30.
- Davies, G.R., Smith Jr., L.B.**, 2006. Structurally controlled hydrothermal dolomite reservoir facies: An overview. *AAPG* 90 (1), 1641–1690.
- Debruyne, D., Hulsbosch, N., Muchez, P.**, 2016. Unraveling rare earth element signatures in hydrothermal carbonate minerals using a source-sink system. *Ore Geol. Rev.* 72, 232–252.
- Deng, Y.X., Ji, Y.L., Xu, S.M., Huang, P., Guo, X.**, 2013. Characteristics and main controlling factors of Tenggeer formation reservoir in Sanghe area, Baiyinchagan sag [in Chinese with English abstract]. *Acta Sedimentol. Sin.* 31 (2), 350–357.
- Diehl, S.F., Hofstra, A.H., Koenig, A.E., Emsbo, P., Christiansen, W., Johnson, C.**, 2010. Hydrothermal zebra dolomite in the Great Basin, Nevada-Attributes and relation to Paleozoic stratigraphy, tectonics, and ore deposits. *Geosphere* 6 (5), 663–690.
- Ebube, A., Karem, A., Nigel, B., Uwe, B., Ihsan, A.**, 2013. Origin of Lower Ordovician dolomites in eastern Laurentia: Controls on porosity and implications from geochemistry. *Mar. Petr. Geol.* 40, 99–114.
- Epstein, S., Buchsbaum, R., Lowenstam, H., Uery, H.C.**, 1953. Revised carbonate-water isotopic temperature scale. *Bull. Geol. Soc. Am.* 64 (11), 1315–1326.
- Fan, M.T., Yang, L.K., Fang, G.Y., Wang, M.F., Li, T.F., Zhu, L.D.**, 2003. Origin of lacustrine hydrothermal sedimentary rock (Lower Cretaceous) in Qingxi sag and its significance [in Chinese with English abstract]. *Acta Sedimentol. Sin.* 21 (4), 560–564.
- Feng, M.Y., Wu, P.C., Qiang, Z.T., Liu, X.H., Duan, Y., Xia, M.L.**, 2017. Hydrothermal dolomite reservoir in the Precambrian Dengying Formation of central Sichuan Basin, Southwestern China. *Mar. Petr. Geol.* 82, 206–219.
- Gawthorpe, R.L., Leeder, M.R.**, 2000. Tectono-sedimentary evolution of active extensional basin. *Basin Res.* 12 (3–4), 195–218.
- Graham, R., Davies, G.R., Smith Jr., L.B.**, 2006. Structurally controlled hydrothermal dolomite reservoir facies: An overview. *AAPG Bull.* 90 (11), 1641–1690.
- Gudmundsson, A., Berg, S., Lyslo, K.B., Skurtveit, E.**, 2001. Fracture networks and fluid transport in active fault zone. *J. Struct. Geol.* 23, 343–353.

- Guo, Q., Zhong, D.K., Zhang, F.D., Liu, X.G., Fan, L.X.,** 2012. Origin of the Lower Cretaceous lacustrine dolostones in Baiyinchagan Sag of Erlian Basin, Inner Mongolia [in Chinese with English abstract]. *J. Palaeogeogr.* 14 (1), 59–68.
- Guo, Q., Li, Z.Y., Qin, M.K., Zhong, D.K., Zhang, F.D.,** 2014. Discussion of hydrothermal sedimentary sequence in Baiyinchagan Sag of Erlian basin, Inner Mongolia [in Chinese with English abstract]. *Acta Sedimentol. Sin.* 32 (5), 809–813.
- Guo, C., Chen, D.Z., Qing, H.R., Dong, S.F., Li, G.R., Wang, D., Qian, Y.X., Liu, C.,** 2016. Multiple dolomitization and later hydrothermal alteration on the Upper Cambrian–Lower Ordovician carbonates in the northern Tarim Basin, China. *Mar. Petr. Geol.* 72, 295–316.
- Hanor, J.S.,** 1994. Origin of saline fluids in sedimentary basins. *Geol. Soc. London, Spec. Publ.* 78 (1), 151–174.
- Hardie, L.A.,** 1987. Dolomitization: A critical view of some current views. *J. Sediment. Petrol.* 57, 166–183.
- Hendry, J.P., Gregg, J.M., Shelton, K.L., Somerville, I.D., Crowel, S.F.,** 2015. Origin, characteristics and distribution of fault-related and fracture-related dolomitization: Insights from Mississippian carbonates, Isle of Man. *Sedimentology* 62 (3), 717–752.
- Heydari, E.,** 1997. The role of burial diagenesis in hydrocarbon destruction and H<sub>2</sub>S accumulation, Upper Jurassic Smackover Formation, Black Creek Field, Mississippi. *AAPG Bull.* 81 (1), 26–45.
- Hu, W.S., Lei, Z.C., Xu, C., Liu, T.J., Xu, B.,** 2013. Study on dolomite reservoir of Xilinhaolai oilfield in Baiyinchagan depression [in Chinese with English abstract]. *Spec. Oil Gas Reservoir* 20 (1), 11–14.
- Huang, H.P., Jin, G.X., Lin, C.S., Zheng, Y.B.,** 2003. Origin of an unusual heavy oil from the Baiyinchagan depression, Erlian basin, northern China. *Mar. Petr. Geol.* 20, 1–12.
- Karem, A., Denis, L., Lan, K., Guo X.C.,** 2008. Dolomitization of the Lower Ordovician Aguathuna Formation carbonates, Port au Port Peninsula, western Newfoundland, Canada: implications for a hydrocarbon reservoir. *Can. J. Earth Sci.* 45, 795–813.
- Keith, M.H., Weber, J.N.,** 1963. Isotopic composition and environmental classification of selected limestone and fossils. *Geochim. Cosmochim. Acta* 28, 259–260.
- Liu, C.X., Zhang, X.H.,** 2011. Relationship between paleo-geotherm and hydrocarbon generation in the Baiyinchagan depression, Erlian basin [in Chinese with English abstract]. *J. Shandong University Sci. Technol.* 30 (3), 12–20.
- Liu, H., Ma, T., Tan, X.C., Zeng, W., Hu, G., Xiao, D., Luo, B., Shan, S.J., Su, C.P.,** 2016. Origin of structurally controlled hydrothermal dolomite in epigenetic karst system during shallow burial: An example from Middle Permian Maokou Formation, central Sichuan Basin, SW China. *Petr. Explor. Dev.* 43 (6), 1000–1012.
- Li, Q., Jiang, Z.X., Hu, W.X., You, X.L., Hao, G.L., Zhang, J.T., Wang, X.L.,** 2016. Origin of dolomites in the Lower Cambrian Xiaoerbulak Formation in the Tarim Basin, NW China: Implications for porosity development. *J. Asian Earth Sci.* 115, 557–570.
- Liu, S.G., Huang, W.M., Jansa, L.F., Wang, G.Z., Song, G.Y., Zhang, C.J., Sun, W., Ma, W.X.,** 2014. Hydrothermal dolomite in the Upper Sinian (Upper Proterozoic) Dengying Formation, East Sichuan Basin, China. *Acta Geol. Sin.* 88 (5), 1466–1487.
- Liu, Y.Q., Jiao, X., Li, H., Yuan, M.S., Yang, W., Zhou, X.H., Liang, H., Zhou, D.W., Zheng, C.Y., Sun, Q., Wang, S.S.,** 2012. Primary dolostone formation related to mantle-originated exhalative hydrothermal activities, Permian Yuejingou section, Santanghu area, Xinjiang, NW China. *Sci. China, Ser. D Earth Sci.* 55 (2), 183–192.
- Mazzullo, S.J.,** 1981. Facies and burial diagenesis of a carbonate reservoir: Chapman Deep (Atoa) Field Delaware Basin, Texas. *AAPG* 65, 850–865.
- Mazzullo, S.J., Harris, P.M.,** 1992. Mesogenetic dissolution: Its role in porosity development in carbonate reservoir. *AAPG* 76 (5), 607–620.
- Morrow, D.W.,** 2014. Zebra and boxwork fabrics in hydrothermal dolomites of northern Canada: Indicators for dilational fracturing, dissolution or in situ. *Can. Soc. Petr. Geol.* 61 (4), 915–951.
- Qing, H.R., Mountjoy, E.W.,** 1994. Formation of coarsely crystalline, hydrothermal dolomite reservoirs in the Presqu'île barrier, Western Canada sedimentary basin. *AAPG Bull.* 78 (1), 55–77.
- Schellische, R.W.,** 1991. Half-graben basin filling models: New constraints on continental extensional basin development. *Basin Res.* 3 (2), 123–141.
- Scholz, C.A., Hutchinson, D.R.,** 2000. Stratigraphic and structural evolution of the Selenga delta accommodation zone, Lake Baikal rift, Siberia. *Int. J. Earth Sci.* 89 (3), 212–228.
- Schrijver, K., Williams-Jones, A.E., Bertrand, R., Chagnon, A.,** 1996. Genesis and controls of hydrothermal dolomitization in sandstones of the Appalachian thrust belt, Quebec, Canada: Implications for associated galena-barite mineralization. *Chem. Geol.* 129 (3–4), 257–279.

**Slater, B.E., Smith, L.B.**, 2012. Outcrop analog for Trenton–Black River hydrothermal dolomite reservoirs, Mohawk Valley, New York. *AAPG Bull.* 96 (7), 1369–1388.

**Wen, H.G., Zheng, R.C., Wu, G.X., Xia, P.F., Chen, H.R.**, 2009. Characteristics of strontium isotopic geochemistry of sublacustrine hydrothermal sedimentary rock of Xiagou Formation in Qingxi sag, Jiuquan Basin [in Chinese with English abstract]. *Acta Sedimentol. Sin.* 27 (4), 642–649.

**Wen, H.G., Zheng, R.C., Qing, H.R., Fan, M.T., Li, Y.A., Gong, B.S.**, 2013. Primary dolostone related to the Cretaceous lacustrine hydrothermal sedimentary in Qingxi sag, Jiuquan Basin on the northern Tibetan Plateau. *Sci. China, Ser. D Earth Sci.* 56 (12), 2080–2093.

**Wang, J.H., Zou, C.N., Jin, J.Q.**, 2011. Characteristics and controlling factors in igneous rock reservoirs [in Chinese with English abstract]. *Pet. Explor. Dev.* 38 (6), 708–715.

**Wang, L.Z., Wang, D.R., Wang, L.Z.**, 1995. Source-reservoir-cap characteristics and its hydrocarbon accumulation of Cretaceous in Baiyinchagan depression [in Chinese with English abstract]. *Fault-Block Oil Gas Field* 2 (2), 29–34.

**Xu, S.T., Zhang, H.B., Zhang, T.Z.**, 2005. Reservoir diagenesis and its vertical zoning of Baiyinchagan depression. *Petr. Geol. Oilfield Dev. Daqing* 24 (5), 4–7.

**Xu, Y.T., Shang, S.C., Zhang, B.H.**, 2000. Evidence for metallogenic geochemistry of volcano-hot spring deposition in Xiqiu Copper Massive Sulfide Deposit, Zhejiang Province [in Chinese with English abstract]. *Geochimica* 29 (1), 14–20.

**Yuan, J.Y., Huang, C.G., Zhao, F., Pan, X.**, 2015. Carbon and oxygen isotopic compositions, and palaeoenvironmental significance of saline lacustrine dolomite from the Qaidam Basin, Western China. *J. Petr. Sci. Engin.* 135, 596–607.

**Yue, X.D., Lin, C.M., Li, Y.L., Xu, S.M., Zhang, Z.P.**, 2009. The discovery of seismites in the lower Cretaceous of Baiyinchagan depression, Erlian Basin and its geological implications [in Chinese with English abstract]. *Geol. J. China Universities* 15 (1), 57–62.

**Zeng, L.B.**, 2010. Microfracturing in the Upper Triassic Sichuan Basin tight-gas sandstones: Tectonic, overpressure, and diagenetic origins. *AAPG Bull.* 92 (12), 1811–1825.

**Zhang, F.S.**, 2005. Fan delta and braided delta sediments in Baiyinchagan depression [in Chinese with English abstract]. *Acta Geosci. Sin.* 26 (6), 553–556.

**Zhang, F.S., Wang, S.L., Sun, Y.P., Zhang, F.D.**, 2003. Framework of sequence stratigraphy and filling style of Baiyinchagan sag [in Chinese with English abstract]. *Petr. Explor. Dev.* 30 (4), 32–33.

**Zheng, R.C., Wang, C.S., Zhu, L.D., Liu, H.J., Fang, G.Y.**, 2003. Discovery of the first example of “White smoke type” of exhalative rock (hydrothermal sedimentary dolostone) in Jiuxi Basin and its significance [in Chinese with English abstract]. *J. Chengdu University Technol. (Science and Technology Edition)* 30 (1), 1–8.

**Zhu, D.Y., Meng, Q.Q., Jin, Z.J., Liu, Q.Y., Hu, W.X.**, 2015. Formation mechanism of deep Cambrian dolomite reservoirs in the Tarim Basin, northwestern China. *Mar. Petr. Geol.* 59, 232–244.

**Zuo, Y.H., Wang, C.C., Tang, S.L., Hao, Q.Q.**, 2016. Mesozoic and Cenozoic thermal history and source rock thermal evolution of the Baiyinchagan sag, Erlian Basin, Northern China. *J. Petr. Sci. Engin.* 139, 171–184.

*Рекомендована к печати 20 сентября 2017 г.  
Н.В. Сенниковым*

*Поступила в редакцию 16 ноября 2016 г.,  
после доработки — 19 июля 2017 г.*